Phonon coupling effects in proton scattering from ^{40}Ca

R. S. Mackintosh*
Department of Physical Sciences, The Open University, Milton Keynes, MK7 6AA, United Kingdom

N. Keeley†
National Centre for Nuclear Research, ul. Andrzeja Sołtana 7, 05-400 Otwock, Poland

(Received 24 June 2014; revised manuscript received 12 September 2014; published 2 October 2014)

Background: Formal optical model theory shows that coupling to vibrational nuclear states generates a nonlocal and l-dependent dynamical polarization potential (DPP). Little is established concerning the DPP, yet its properties are crucial for explaining the departures of optical model potentials (OMPs) from global behavior and for the rigorous extraction of spectroscopic information from direct reactions.
Purpose: To appraise the application of channel coupling followed by S-matrix inversion for the systematic exploration of the contribution of the coupling of collective states to the nucleon OMP and to identify properties of nuclear potentials indicative of l-dependence.
Methods: S-matrix to potential, $S_{lj} \rightarrow V(r) + \mathbf{l}\cdot\mathbf{s}\ V_{\rm SO}(r)$, inversion provides local potentials that precisely reproduce the elastic channel S-matrix from coupled channel (CC) calculations. Subtracting the elastic channel uncoupled (bare) potential yields a local and l-independent representation of the DPP. The dependence of this local DPP upon the nature of the coupled states and upon other parameters can be studied.
Results: All components of the DPP arising from coupling to vibrational states are substantially undulatory with a point-by-point magnitude therefore disproportionate to their contribution to volume integrals. Information relating to dynamical nonlocality is found. The proton charge leads to a substantial difference between DPPs for protons and neutrons.
Conclusions: Undulatory features in potentials found in precision fits to elastic scattering data are significant, are a consequence of coupling to inelastic channels and must be allowed for in phenomenology; they are indirect evidence of l-dependence. Within the model, coupling to excited states magnifies the effect of the proton charge on the difference between proton-nucleus and neutron-nucleus interactions. Coupled channel plus inversion is a procedure of wide applicability, complementary to evaluation of the Feshbach formalism.

DOI: 10.1103/PhysRevC.90.044601 PACS number(s): 25.40.Cm, 24.10.Ht, 24.10.Eq, 02.30.Zz

I. INTRODUCTION

Pignanelli *et al.* [1] (hereafter PGL) showed that the explicit coupling to a giant quadrupole resonance (GQR) state improved the fit to the backward angle differential cross section for proton scattering from ^{40}Ca at 30.3 MeV. The data in question have never been fitted with smooth potentials of standard parameterized forms. Potentials that fitted these data required unconventional features: l-dependence [2–5] or undulatory character [6,7]. The need for these unconventional models for nucleon elastic scattering has not been widely accepted because of the deceptive ease with which the generally available elastic scattering data for many (but not all; see Ref. [8]) non-closed-shell nuclei can be reasonably well fitted with standard radial forms. We note that there have been other calculations [9], similar to those of PGL, that have included low-energy phonons. The coupling of proton elastic scattering to deuteron channels also has a considerable effect on the angular distribution, and local potentials having the same elastic channel S-matrix S_{lj} are undulatory [10]. In the past, attempts have been made [11] to relate l-dependence, or the undulatory nature of potentials that precisely fit high-quality data, to reaction coupling or collective coupling, but the understanding is very incomplete.

Fitting data like that mentioned above evidently requires physics beyond the highly developed [12–15] local density model. Such models would not seem to have any place for angular momentum dependence, for example. The aim of this work is to demonstrate, with examples involving the coupling to vibrational states, how S-matrix inversion can be exploited to uncover implications for elastic nucleon scattering phenomenology of processes that are not well represented by local density models. Section II presents and discusses the local potentials equivalent to the coupling of PGL. Section III presents contrasting results for more general couplings for the same scattering case, and the final section draws general conclusions.

II. DPP DUE TO THE GQR

In what follows, we produce local and l-independent potentials that give exactly the same elastic scattering angular distributions as were found in the coupled channels (CC) calculations of PGL that included the GQR. This is done by applying $S_{lj} \rightarrow V(r) + \mathbf{l}\cdot\mathbf{s}\ V_{\rm SO}(r)$ inversion [16–18] to the elastic channel S-matrix output by the CC code FRESCO [19]. The local, l-independent dynamic polarization potential (DPP) generated by the coupling is obtained by subtracting the

*raymond.mackintosh@open.ac.uk
†keeley@fuw.edu.pl

TABLE I. For protons scattering from ^{40}Ca at indicated values of MeV/nucleon in column 1, characteristics of the bare potentials. For each energy, σ^{A}_{Reac} is the reaction cross section with potential A.

E (lab.)	Pot.	J_R	R_R(rms)	J_I	R_I(rms)	σ_{Reac} (mb)	σ^{A}_{Reac} (mb)
All	A	400.30	4.0096	100.42	5.0028		
20.0	B	440.35	4.1189	52.17	4.1661	703.93	924.53
30.3	B	413.21	4.1189	65.73	4.1314	695.26	882.60
60.0	B	334.94	4.1189	49.28	3.7773	429.94	774.31
90.0	B	255.88	4.1189	50.18	3.4834	343.66	654.21

elastic channel ("bare") potential used in the CC calculation from the potential found by inversion. Key properties in the following discussion are the changes induced by the coupling in J_R, J_I, R_R(rms), and R_I(rms), respectively, the real and imaginary volume integrals (conventionally defined in Ref. [20]) of the central potential and the real and imaginary rms radii. The changes induced in the volume integrals such as ΔJ_R, i.e., the volume integrals of the DPP, are simply the differences between the volume integrals of the inverted and bare potentials. The effects of the coupling on the spin-orbit terms are conveyed graphically only.

To facilitate comparison with the results of PGL, we employ potentials used by them and adopt the same GQR state of ^{40}Ca: a 2^+ at 18.5 MeV, using vibrational model coupling with the same deformation length, $\delta = \beta_\lambda R$ for each component of the potential. The first set of calculations were carried out with potential set 1 of Table I of PGL evaluated at 30.3 MeV, so this potential was fixed for all energies studied; we refer to this as potential A. The second choice of bare potential was set 3 of PGL, evaluated for each energy according to the energy dependence given in PGL Table I; we refer to this as potential B. This potential has a Gaussian imaginary term having a volume integral at 30.3 MeV $J_I = 65.73$ MeV fm^3, much less than predicted for global potentials; it is similarly low at the other energies considered.

The use of both fixed and energy-dependent bare potentials, which were substantially different even at 30.3 MeV, will provide information concerning the sensitivity of the DPPs, and also the elastic scattering observables, to differences in the bare potential. In particular, potential A reveals the part of the energy dependence of the DPP that does not arise from the energy dependence of the bare potential. Potential B is not, in fact, very realistic over the range of energies for which it is applied here. The characteristics of these potentials are presented in Table I together with the reaction cross sections without coupling, σ_{Reac}. The quantity σ^{A}_{Reac} in the last column is the no-coupling reaction cross section for the fixed potential A. Unsurprisingly, there is an increasing divergence between σ_{Reac} and σ^{A}_{Reac} at the higher energies.

The characteristics of the DPP for each energy are presented in Table II. Column 7 gives the change in reaction cross section (CS), $\Delta\sigma_r$, induced by the coupling, and column 8 gives the inelastic cross section σ_{inel} to the GQR. In all these cases $\Delta\sigma_r$ is positive although there are many cases, see Ref. [21], where inelastic or reaction-channel coupling reduces the reaction CS. For 30.3 MeV, Pot A, the coupling to the GQR increases the

TABLE II. For protons scattering from ^{40}Ca at indicated values of MeV/nucleon. The bare potential is indicated in column 2, with A fixed and B energy dependent, as described in the text. Columns ΔJ_R and ΔJ_I give the volume integrals (per nucleon pair) (in MeV fm^3) of the central components of the DPP induced by coupling to the GQR. Negative ΔJ_R corresponds to repulsion. ΔR_R(rms) and ΔR_I(rms) are the changes in rms radius of the real and imaginary central components (in fm). The two final columns present, respectively, the change in the total reaction CS, $\Delta\sigma_r$, induced by the coupling, and the integrated inelastic CS, σ_{inel}, to the specific coupled inelastic channel. The second 30.3 MeV case, indicated by 30.3^{RC}, is for coupling with only the real potential deformed.

E (lab.)	Pot.	ΔJ_R	ΔR_R (rms)	ΔJ_I	ΔR_I (rms)	$\Delta\sigma_r$ (mb)	σ_{inel} (mb)
20.0	A	3.56	0.021	8.65	0.071	11.31	2.13×10^{-4}
20.0	B	19.4	0.065	17.32	0.010	68.71	8.68×10^{-4}
30.3	A	2.24	0.0002	6.51	0.057	19.56	12.75
30.3	B	1.52	0.0008	5.69	0.166	29.42	18.19
30.3^{RC}	A	3.40	0.0135	5.80	0.033	17.63	11.22
60.0	A	1.66	−0.0038	5.31	−0.015	21.36	23.83
60.0	B	0.55	0.0003	3.46	0.0672	22.05	17.45
90.0	A	1.10	−0.0020	4.51	−0.016	17.68	20.25
90.0	B	0.04	0.0014	1.77	0.0399	10.08	9.44

reaction CS σ_r by 19.56 mb, a factor of 1.53 greater than the inelastic scattering CS σ_{inel}. This factor becomes 5.3×10^4 at 20 MeV. The suppression of the inelastic CS at this near-threshold energy is due to the very low energy proton in the exit channel being trapped by the Coulomb barrier. Column 5 of Table I presents J_I for the bare potential, the quantity that differs most between potential A and potential B. Both the Becchetti-Greenlees [22] and Koning-Delaroche [23] global potentials have a much larger value of J_I at the higher energies than potential B.

The DPPs corresponding to the 30.3 MeV case with complex coupling are shown in Fig. 1. The DPP for bare potential A (dashed lines) is generally less wavy than the DPP for the global bare potential B (solid lines), but otherwise they are very similar. The bare potentials are reasonably appropriate at 30.3 MeV, and the difference between the values of J_I for potentials A and B, although substantial, is less than at the other energies. The DPP calculated when only the real OMP is deformed is shown in Fig. 2 where it is compared with the DPP calculated with complex coupling for potential A, also shown in Fig. 1. The DPPs shown in these figures are not large, reflecting the small deformation length of the GQR. As noted by PGL, the crucial modification of the angular distribution at backward angles is accompanied by very small changes at most other angles.

The DPPs for the 20 MeV case with complex coupling are shown in Fig. 3. At this energy, the DPPs for the A and B potentials are very different, not surprisingly in view of the circumstances that lead to an almost zero CS, σ_{inel}, to the GQR state. A quantitative measure of the difference between the A and B DPPs is the large difference in the values of ΔJ_R and ΔJ_I, both being much larger for the B case. This is related to the fact that J_I for the bare potential at 20 MeV

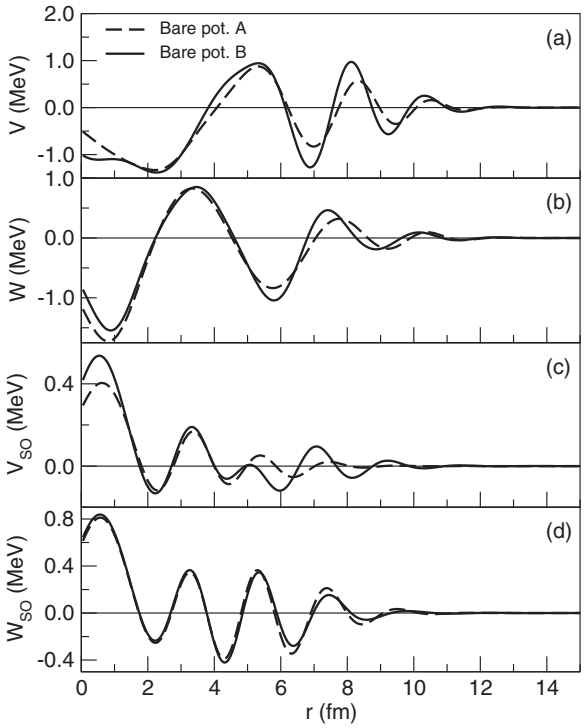

FIG. 1. For 30.3 MeV protons scattering from ^{40}Ca, the DPP calculated with full (complex) coupling to the GQR. The dashed line is for the bare potential A and the solid line is for the global potential B. Panels (a)–(d) are respectively real and imaginary central and real and imaginary spin-orbit terms.

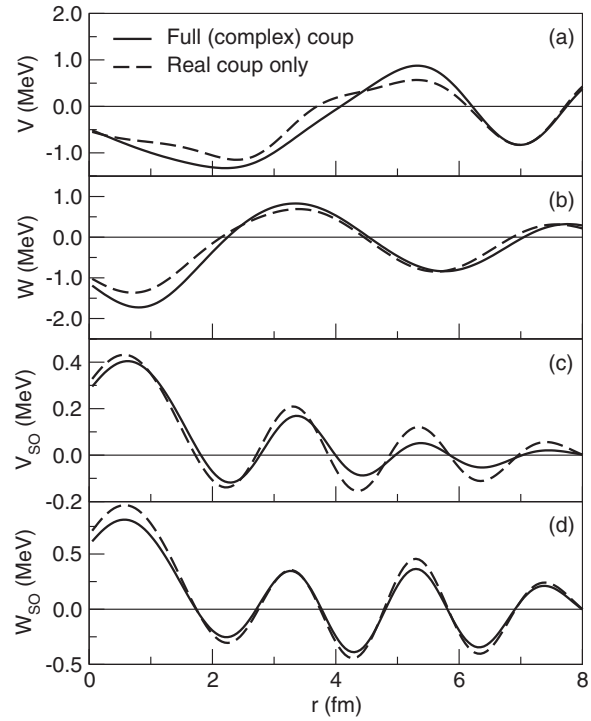

FIG. 2. For 30.3 MeV protons scattering from ^{40}Ca, the DPP calculated with bare potential A. The DPP for full (complex) coupling to the GQR is shown as the solid line and the DPP with real coupling only is the dashed line. Note that the x-axis scale is different from that for Fig. 1, which includes the same complex coupling DPP. Panel labels are as for Fig. 1.

is much greater for A than for B and to the very different values of σ_r with no coupling. The wave function in the nuclear interior is more attenuated in the A case and this is probably why the DPP is attenuated for small r. The large increase in reaction cross section induced by coupling in the B case is almost entirely due to a large decrease in $|S_{lj}|$ for the $9/2^-$ partial wave. Counterintuitive increases in $|S_{lj}|$ resulting from channel coupling are present at 20 and 30.3 MeV for certain partial waves but not at higher energies. See Ref. [21] for a discussion of this phenomenon.

At 60 and 90 MeV, the differences between the A and B values of J_I for the bare potential are also large. The inverted potentials for 20 MeV, and (not shown) for 60 MeV and 90 MeV, calculated with the same bare potential as used at 30.3 MeV, have consistent qualitative features. Coupling makes the real central potential somewhat deeper for $r < 4$ fm and slightly shallower and then undulatory for larger r. The imaginary potential becomes significantly more absorptive at the nuclear center and the radius at which it is deepest is pushed outward. An undulatory feature in the imaginary DPP, shown in Fig. 1, corresponds to an outward shift in the imaginary potential. There is always an absorptive effect at the nuclear center, which is interesting, since this is where the coupling is small.

When coupling is switched on, the increase $\Delta\sigma_r$ includes the inelastic scattering cross section, suggesting that $\Delta\sigma_r$ would be greater than σ_{inel}, and this is the case for the 20 and 30.3 MeV cases but not for potential A at 60 and 90 MeV. This is probably

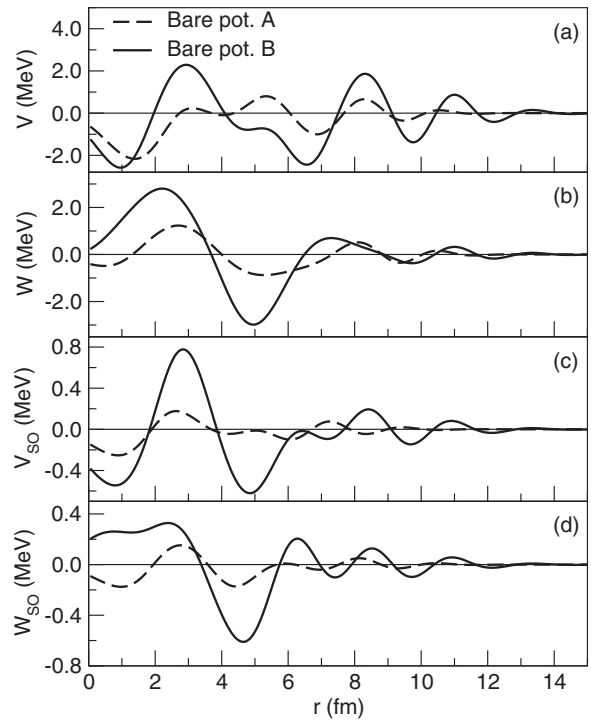

FIG. 3. For 20 MeV protons scattering from ^{40}Ca, the DPP calculated with full (complex) coupling to the GQR. The dashed line is for the bare potential A and the solid line is for the global potential, B. Panel labels are as for Fig. 1.

connected with J_I being greater for the A than the B potential at these energies. This connection is also suggested by the fact that at 30.3 MeV with real coupling $\sigma_{\rm inel}$ and also $\Delta\sigma_{\rm r}$ are smaller than with complex coupling.

III. MORE GENERAL VIBRATIONAL COUPLING

Although PGL found that the GQR had a significant effect on the angular distribution at far backward angles, the volume integrals of the DPP are small although the DPP is not small point by point, especially for the imaginary part. It is therefore of interest to explore the contribution of the many other vibrational states, many with much greater strength than the GQR. For example, it is known, e.g., Ref. [24], that certain low-lying states, such as the 3^- state at 3.737 MeV, make a larger contribution to the OMP. We therefore performed further CC-plus-inversion calculations involving low-lying excitations. For these, the bare potential used Becchetti-Greenlees (BG) [22] parameters. This global potential is not regarded as appropriate for $A = 40$, but is adequate for the purpose of studying contributions that are generally omitted; the BG potential is more realistic than potentials A and B of Ref. [1].

All calculations were for 30.3 MeV protons on ^{40}Ca. In Table III we compare the contributions of coupled vibrational states: (i) the 2^+ state at 3.9 MeV, (ii) a 2^+ state with the same deformation length δ as state (i) at 18.5 MeV, the excitation energy of the GQR, (iii) the GQR at 18.5 MeV, (iv) the 3^- state at 3.737 MeV, and (v) the 3^- state at 3.737 MeV but with the same deformation length δ as the 2^+ state at 3.9 MeV. Some of these states were included together in Ref. [9]. The GQR deformation length δ is that used by PGL, and the deformation lengths for the 3.9 and 3.737 MeV states are realistic. The deformation length δ to the 2^+ test state (ii) is the same as the 3.9 MeV state (i) but has the same excitation energy as the GQR. Test state (v) has the same multipolarity as state (iv) but the same δ as state (i). One surprise: the change in reaction CS is exactly the same for the 2^+ at 3.9 MeV as it is for the test 2^+ at 18.5 MeV and the changes in the real and imaginary volume integrals are surprisingly close. However, the inelastic CS does depend strongly on excitation energy and/or angular momentum transfer. From Table III we also learn that the real and imaginary volume integrals of the DPPs, apart from that for the 3^- state, tend to be small, notwithstanding the significant qualitative effect on the angular distribution as found by PGL for the GQR. The undulatory DPP is not so small point by point, as shown for the the 3^- state at 3.737 MeV in Fig. 4.

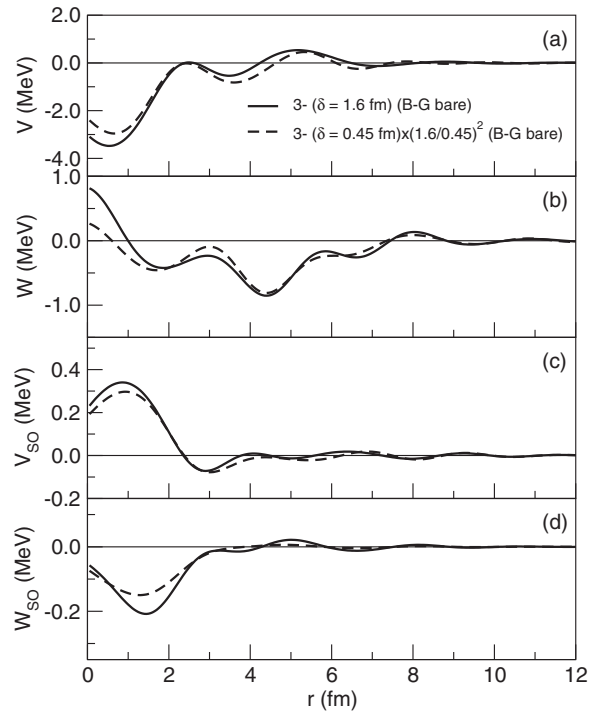

FIG. 4. For 30.3 MeV protons scattering from ^{40}Ca, the solid line is the DPP calculated with full (complex) coupling to the 3^- state at 3.737 MeV and $\delta = 1.6$ fm. The bare potential was the Becchetti-Greenlees global potential. The dashed line is the DPP for $\delta = 0.45$ fm multiplied by $(1.6/0.45)^2$. Panel labels are as for Fig. 1.

In fact, this low-lying state does contribute substantially to the absorptive part of the OMP.

The radial form of the DPP due to a single collective excitation depends upon both the multipolarity and excitation energy. There are too many combinations to compare visually, but in Fig. 5 we compare the DPPs due to a strong low-energy 3^- state (dashed line) with that due to the high-energy GQR (solid line). In this figure both states employ the Becchetti-Greenlees bare potential, unlike the GQR DPP in Fig. 1. The imaginary components of the DPP for the 3^- and GQR excitations are quite different. However, Fig. 5 reveals common features in the real DPP for the GQR and the 3^- state: Both show attraction at the nuclear center and a repulsive bump around 5 fm which, in the case of the 3^- state, leads to a negative (repulsive) $\Delta J_{\rm R}$. In these and all other cases,

TABLE III. For protons scattering from ^{40}Ca at 30.3 MeV, characteristics of cross sections and DPPs when the vibrational coupling to the indicated single state is included, with excitation energies in parentheses. The deformation length is δ. We use $\sigma_{\rm inel}$ for the inelastic scattering cross section and $\Delta\sigma_{\rm r}$ is the change in reaction cross section due to the coupling.

Case	Excitation	δ	$\sigma_{\rm inel}$	$\frac{\sigma_{\rm inel}}{\delta^2}$	$\Delta\sigma_{\rm r}$	$\frac{\Delta\sigma_{\rm r}}{\delta^2}$	ΔJ_R	ΔJ_I	$\frac{\Delta J_R}{\delta^2}$	$\frac{\Delta J_I}{\delta^2}$
(i)	2+ (3.9 MeV)	0.45	4.852	23.96	4.73	23.36	0.50	1.485	2.47	7.33
(ii)	2+ (18.5 MeV, test)	0.45	1.632	8.06	4.73	23.36	0.58	1.585	2.86	7.83
(iii)	2+ (18.5 MeV, GQR)	0.91	6.926	8.36	17.43	21.05	1.05	5.835	1.27	7.05
(iv)	3− (3.737 MeV)	1.6	40.91	15.98	32.96	12.88	− 1.45	12.325	− 0.566	4.814
(v)	3− (3.737 MeV, test)	0.45	3.12	15.41	3.05	15.06	0.35	0.935	1.72	4.617

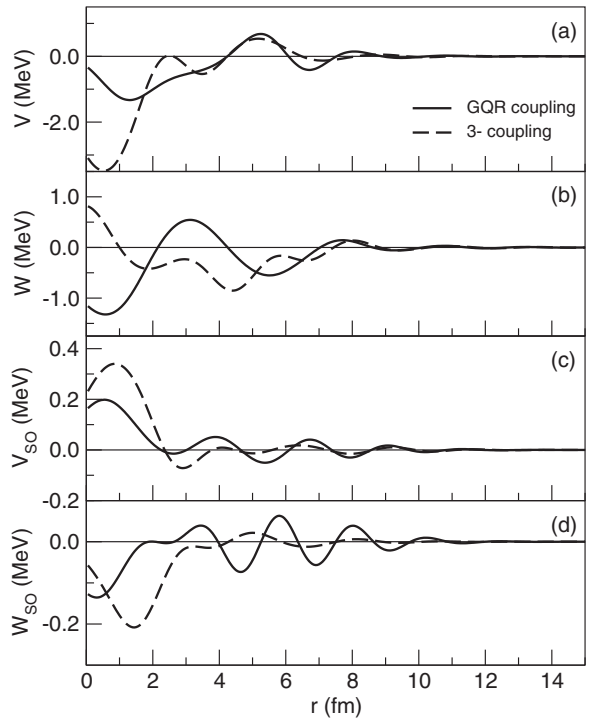

FIG. 5. For 30.3 MeV protons scattering from ^{40}Ca, the solid line is the DPP for the GQR with full complex coupling. The dashed line is the DPP for excitation of the 3^- state at 3.737 MeV and $\delta = 1.6$ fm. In each case the bare potential was the Becchetti-Greenlees global potential. Panel labels are as for Fig. 1.

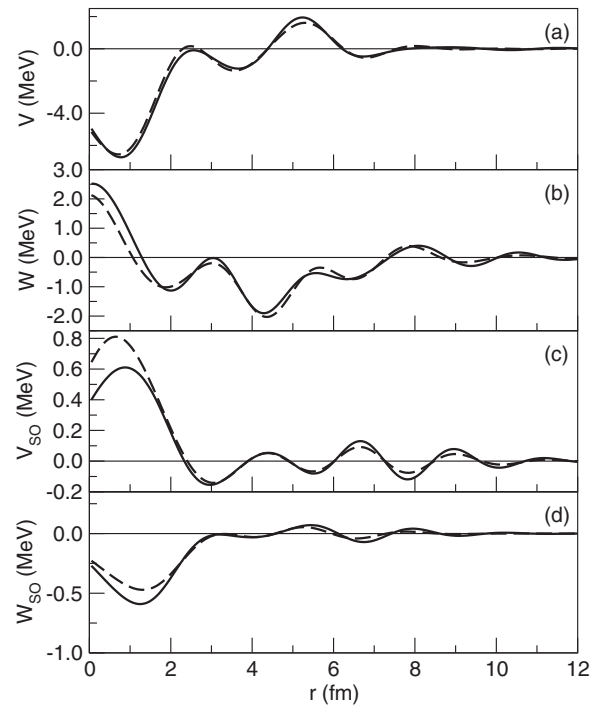

FIG. 6. For 30.3 MeV protons scattering from ^{40}Ca, the solid line is the DPP arising from the coupling to two identical 3^- states at 3.737 MeV with $\delta = 1.6$ fm. The dashed line is a factor of 2 times the DPP for a single 3^- state at 3.737 MeV. Panel labels are as for Fig. 1.

the imaginary DPP has excursions into emissiveness; this is substantial at $r = 0$ for the 3^- case.

The DPPs that we present are local equivalents of the formal nonlocal DPP of Feshbach theory. This dynamical nonlocality is unrelated to exchange nonlocality that generates most of the energy dependence of the nucleon OMP and is responsible for the well-known Perey effect; see Refs. [25,26]. The cases in Table III reveal consequences of the underlying nonlocality such as the different degrees of departure of the real and imaginary DPPs and their volume integrals from the proportionality to deformation length squared, δ^2, that would be expected for the formal nonlocal DPP for phonon coupling. The nonlocality of the underlying nonlocal DPP also manifests itself as follows: For two phonons coupled to the elastic channel but not mutually coupled, the nonlocal DPPs must add. However, local equivalent potentials will not add exactly, and we have performed a model calculation to demonstrate this. Two identical 3^- phonons at 3.737 MeV were coupled to the elastic channel and the DPP was calculated, and in Fig. 6 we compare the DPP due to the two phonons with twice the DPP due to the single phonon. The difference is a manifestation of the nonlocality of the formal DPP. The consequence of this dynamical nonlocality for direct reactions will be discussed in a subsequent publication. Differences between the radial form of the DPP due to the 3^- state, evident in a close comparison of Figs. 4 and 6, are a consequence of slightly different forms of inelastic coupling as specified below in connection with Table IV.

The contribution of the 3^- state to the real DPP is apparently nonlinear, with the negative ΔJ_R indicating overall repulsion for a realistic deformation length. However, the comparison in Fig. 4 of the DPP with the DPP calculated with the much smaller δ and scaled by δ^2 shows that the response is more linear than that would suggest, with the negative ΔJ_R arising from the repulsive bump near 5 fm. The fact that the local DPP shown in Fig. 4 does not scale with δ^2 is a manifestation of the nonlocality of the formal DPP. The local equivalent of $\alpha\times$ a nonlocal potential is not $\alpha\times$ the local equivalent of the original nonlocal potential. Comparing $\Delta J_R/\delta^2$ and $\Delta J_I/\delta^2$ for cases (ii) and (iii) and also for cases (iv) and (v) reveals a

TABLE IV. Comparing the contribution of the 3^- vibrational state to the scattering of protons and neutrons from ^{40}Ca at 30.3 MeV. The volume integrals of the DPPs and changes to rms radii occur when the vibrational coupling is included. For protons we present the cases both with and without Coulomb excitation (couex). We use σ_{inel} for the inelastic scattering cross section and $\Delta\sigma_r$ is the change in total reaction cross section due to the coupling.

Quantity	Neutrons	Protons (no couex)	Protons (couex)
ΔJ_R	− 1.34	− 1.69	− 1.62
ΔR_R	− 0.0198	− 0.0227	− 0.0211
ΔJ_I	13.14	14.23	13.125
ΔR_I	0.0221	0.0376	0.0326
$\Delta\sigma_r$	42.8 mb	36.06 mb	33.33 mb
σ_{inel}	53.11 mb	46.33 mb	43.57 mb

much more linear response for the imaginary part than for the real part. Comparison of the same two pairs of cases reveals that both the inelastic and reaction cross sections are roughly linear in δ^2, unlike ΔJ_R. A comparison of lines (i) and (v) suggests that a larger angular momentum transfer is associated with both a smaller DPP and smaller inelastic and reaction cross sections. For the lower energy excitations, but not for the GQR at 18.5 MeV, $\sigma_{\rm inel}$ exceeds $\Delta\sigma_r$, so the collective coupling reduces the remaining absorptive contribution to the reaction cross section.

Inversion shows that differences between proton and neutron OMPs can occur as an indirect consequence of the Coulomb interaction. Table IV compares characteristics of the DPPs arising in proton and neutron scattering from the coupling to the 3^- state at 3.737 MeV. For protons, there are cases both with and without Coulomb excitation. In the absence of Coulomb excitation, the differences in DPP, $\Delta\sigma_r$, and $\sigma_{\rm inel}$ arise solely from the central Coulomb interaction of the proton; the mass difference has a negligible effect and the same bare potential and coupling interactions are used for both projectiles. Concerning the proton cases, we remark that slight differences in ΔJ_R and ΔJ_I from those in line (iv) of Table III are the result of a slightly different form of inelastic coupling to the vibrational state.

The calculations can be extended to include many vibrational states. An obvious question is would a more realistic collection of phonon excitations lead to an averaging out of the oscillatory features? Smoother potentials would be consistent with Woods-Saxon phenomenology and folding models based on the local density approximation, e.g., Refs. [12,13]. To investigate this, we calculated, ignoring proton spin, the contribution of an array of 10 vibrational states of multipolarities ranging from dipole, 1^-, to 5^-, and excitation energies up to 18 MeV. The vibrational states are those selected by Coulter and Satchler [24] and were coupled with their deformation lengths. Unlike most of the Ref. [24] calculations, we have included a small central imaginary term in the bare potential, with the same geometry as the real component, in part to represent the coupling to pickup channels. The bare potential did not depend upon the energy of the nucleons in the excited-state channels. Pickup coupling was included in Ref. [24] but is not included in the present calculations. There were no multiple phonon excitations and no coupling between excited channels justifying some absorption in the bare potential.

Alongside the proton calculations, we carried out identical calculations for neutrons. In addition, proton calculations with no Coulomb excitation were performed in order to identify those differences in the DPP that are entirely due to the presence of an undeformed Coulomb potential. The inversion of the resulting S_l gave the DPPs shown in Fig. 7. Apart from in the far surface region, the solid and dashed lines (proton DPPs pot2 and pot3b) follow each other closely, as do the dotted and dot-dashed (neutron DPPs potm5 and pot6) lines. The labels "pot2," "pot3b," "potm5," and "pot6" refer to different inversions as explained below. Characteristics of the same four inverted potentials are presented in Table V, which quantifies the difference between the proton and neutron DPPs. Further substantial differences between the proton and neutron cases occur in the increase in the reaction cross section

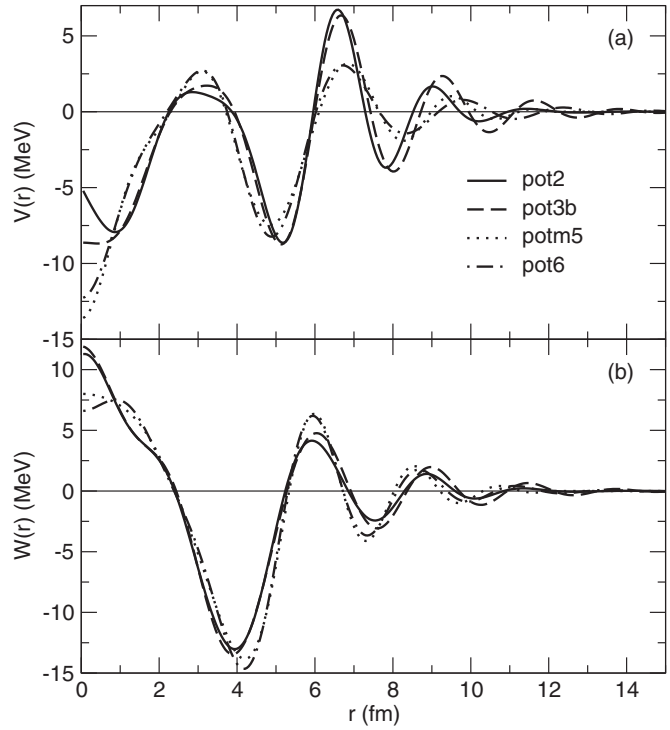

FIG. 7. For 30.3 MeV protons and neutrons scattering from ^{40}Ca, the DPPs arising from the coupling to ten phonons. The solid and dashed lines repesent DPPs for two alternative inversion solutions for protons, and the dotted and dot-dashed lines represent DPPs for two alternative inversion solutions for neutrons. Panel (a) gives the real part and panel (b) gives the imaginary part.

due to the coupling, $\Delta\sigma_r$, and in the summed inelastic cross section, $\sigma_{\rm inel}$. It is unclear why the ratio $\Delta\sigma_r/\sigma_{\rm inel}$ is 1.68 for neutrons and 1.23 for protons, a difference that is unrelated to inversion. In the earlier case of the single 3^- excitation, see Table IV, both $\Delta\sigma_r$ and $\sigma_{\rm inel}$ were greater for neutrons than for protons, unlike the present case. A significant difference was that the imaginary potential in the 3^- case was of global

TABLE V. The contribution of 10 vibrational states to the scattering of protons and neutrons from ^{40}Ca at 30.3 MeV. Characteristics of two inverted potentials for neutrons (potm5 and pot6) and two for protons (pot2 and pot3b) are presented, as in the text. Real and imaginary volume integrals (in MeV fm^3) of the DPPs are presented as are differences in rms radii (in fm), ΔR_R and ΔR_I, between inverted and bare potentials. $\Delta\sigma_r$ is the change in total reaction cross section due to the coupling and $\sigma_{\rm inel}$ is the summed inelastic scattering cross section to the 10 states.

Quantity	Neutron potm5	Neutron pot6	Proton pot2	Proton pot3b
ΔJ_R	52.95	53.62	38.24	39.15
ΔR_R	0.043	0.052	−0.0016	0.0244
ΔJ_I	91.74	90.71	75.45	72.68
ΔR_I	0.1406	0.0911	−0.3454	−0.5757
$\Delta\sigma_r$	638.7 mb	638.7 mb	533.2 mb	533.2 mb
$\sigma_{\rm inel}$	379.3 mb	379.3 mb	431.9 mb	431.9 mb

potential strength. When high-energy target states are excited, the effect of the Coulomb potential for protons is enhanced by the corresponding low energy of the protons. This deserves study as a contribution to the difference between proton and neutron OMPs.

Concerning the two independent solutions for each case, the waviness of the DPP leads to some ambiguity in the $S_l \rightarrow V(r)$ inversion, with a tendency for the undulations, especially in the nuclear surface, to become more marked with increasing precision with which S_l is reproduced. In particular the surface undulations introduce uncertainties into the evaluation of volume integrals and (especially) rms radii. Each pair of solutions represents two different compromises between the amplitude of the undulations in the surface region and the precision of the fit to S_l. For protons the solutions are labeled "pot2" and "pot3b" and for neutrons "potm5" and "pot6." In each case, the second listed potential has a lower value of the S-matrix distance σ, as defined in Ref. [18]; i.e., it fits S_L more closely, together with somewhat greater undularity. All four inverted potentials lead to angular distributions that are graphically indistinguishable from those given directly by the S-matrix from the relevant CC calculation.

We have shown that coupling to the 10 vibrational states did not lead to a smooth DPP due to any averaging effect when many undulatory contributions are added. Therefore, the summed effect of the coupling to multiple vibrational states, where there is no coupling between these states, yields a DPP with strong undulations. Within a model based on the excitation of vibrational states, the coupling between all pairs of states, and also the coupling to multiple phonon multiplets, is a challenge for the future. Although the coupling between any two states involves both the annihilation and creation of phonons, it is acknowledged that there are many such pairs. We note that, as a result of dynamical nonlocality, the individual contributions of phonons do not add precisely, so the addition of the contributions from 10 separate collective excitations would not precisely add to the DPP for all 10 included together, as we have presented.

IV. CONCLUSIONS

The highly nonlocal and l-dependent nature of the contribution of phonon coupling is indicated in the work of Rawitscher [27] and others, e.g., Ref. [24], who begin with the Feshbach expressions [28]. However, that work is not easily related to local optical potential phenomenology and the differential cross sections to the inelastic channels cannot be easily monitored as they can with coupled channel calculations followed by inversion of the elastic scattering S-matrix.

We have shown that the application of exact $S_{lj} \rightarrow V(r) + \mathbf{l}\cdot\mathbf{s}\, V_{\rm SO}(r)$ inversion [16–18] relates coupling effects to local potential phenomenology. We first presented a local potential model of realistic GQR coupling that improved the fit to angular distribution data in a specific case. The undulations in this realistic case raised the question of the effect of more general vibrational couplings. We showed that a justifiable collection of vibrational states leads to strong undulations having an amplitude disproportionate to the effect on $J_{\rm R}$, therefore contributing much less to the energy dependence of the real term than knock-on exchange. The relationship of the undulatory nature of the local equivalent DPP to the nonlocality and l-dependence of the underlying formal DPP, and the consequences of this relationship for direct reactions employing optical potentials in their analysis, are subjects of previous [29] investigations as well as our own ongoing investigations. The determination of DPPs by inversion is highly generalizable since CC calculations can include (i) coupling between inelastic channels, (ii) coupling to reaction channels, and, in principle, (iii) exchange processes, although none of these are included in the calculations reported here.

The present approach is complementary to the highly developed folding model, e.g., [12–15], incorporating a local density, LD, model. As remarked by Köhler [30] in the context of core polarization in shell model calculations, particle-hole excitations are allowed in finite systems. Models in which elastic scattering is treated as a reaction involving a nucleon in the continuum interacting with a finite nucleus, taking into account the specific properties of that nucleus, are much less well developed than LD folding models. However, reaction models open up the possibility of angular momentum dependence, which does not arise naturally within current LD models. It is known that l-dependent potentials have undulatory l-independent S-matrix equivalents. There is evidence for the inconvenient existence of l-dependence; this becomes most apparent with closed shell target nuclei for which deep minima in elastic scattering angular distributions are less obscured. The consistent patterns revealed in the various undulatory potentials presented here, and the specific discussion of alternative potentials in the 10-phonon case, leave no room for dismissal of the existence of undulatory effects as an artefact of the inversion procedure.

Specific results and conclusions of this study include the following:

(i) The effect of GQR coupling, that had been found to correct the backward angle angular distribution in a well-known intransigent case, can be represented by a local and l-independent but undulatory potential.

(ii) The generation of undulatory DPPs by collective coupling is a general feature. The dependence of the DPP upon multipolarity and excitation energy was explored; evidence for dynamical nonlocality was presented; and various features such as different nonlinear responses of the real and imaginary volume integrals were found. The procedure is highly generalizable and presents an opportunity for revealing a rich range of phenomena.

(iii) The undulatory nature of the DPPs accounts for the fact that the effect of collective coupling on scattering is disproportionate to the contribution to volume integrals and the overall energy dependence of the nucleon OMP.

(iv) Within the specific model used, that omits coupling between inelastic excitations, the inclusion of many coupled excitations does not lead to a smooth DPP through an averaging effect.

(v) Collective excitations generate a difference between proton and neutron potentials for $N = Z$ target nuclei.

Final remarks: Why are (apparently) satisfactory optical model potentials not more undulatory? The present work suggests that the exact fitting of precise and wide angular range elastic scattering data, using model-independent methods, leads to undulatory (wavy) potentials which are not necessarily artifacts of the fitting procedure, but reflect true physical phenomena. Fitting high-quality elastic scattering data (usually approximately) by means of uniform renormalization of folding model potentials effectively discards information contained in the data, information concerning the processes described in the present work.

[1] M. Pignanelli, H. V. von Geramb, and R. De Leo, Phys. Rev. C **24**, 369 (1981).
[2] R. S. Mackintosh and L. A. Cordero-L, Phys. Lett. B **68**, 213 (1977).
[3] A. M. Kobos and R. S. Mackintosh, J. Phys. G: Nucl. Phys. **5**, 97 (1979).
[4] A. M. Kobos and R. S. Mackintosh, Acta Phys. Polon. B **12**, 1029 (1981).
[5] J. P. Delaroche, M. S. Islam, and R. W. Finlay, Phys. Rev. C **33**, 1826 (1986).
[6] A. M. Kobos and R. S. Mackintosh, Ann. Phys. (N.Y.) **123**, 296 (1979).
[7] R. Alarcon, J. Rapaport, and R. W. Finlay, Nucl. Phys. A **462**, 413 (1987).
[8] S. Mellema, R. W. Finlay, F. S. Dietrich, and F. Petrovich, Phys. Rev. C **28**, 2267 (1983).
[9] G. M. Honoré, W. Tornow, C. R. Howell, R. S. Pedroni, R. C. Byrd, R. L. Walter, and J. P. Delaroche, Phys. Rev. C **33**, 1129 (1986).
[10] R. S. Mackintosh and N. Keeley, Phys. Rev. C **85**, 064603 (2012).
[11] R. S. Mackintosh and A. M. Kobos, J. Phys. G: Nucl. Part. Phys. **5**, 359 (1979).
[12] E. Bauge, J. P. Delaroche, and M. Girod, Phys. Rev. C **63**, 024607 (2001).
[13] H. F. Arellano and E. Bauge, Phys. Rev. C **84**, 034606 (2011).
[14] R. J. Charity, J. M. Mueller, L. G. Sobotka, and W. H. Dickhoff, Phys. Rev. C **76**, 044314 (2007).
[15] M. H. Mahzoon, R. J. Charity, W. H. Dickhoff, H. Dussan, and S. J. Waldecker, Phys. Rev. Lett. **112**, 162503 (2014).
[16] V. I. Kukulin and R. S. Mackintosh, J. Phys. G: Nucl. Part. Phys **30**, R1 (2004).
[17] R. S. Mackintosh, arXiv:1205.0468.
[18] R. S. Mackintosh, Scholarpedia **7**, 12032 (2012).
[19] I. J. Thompson, Comput. Phys. Rep. **7**, 167 (1988).
[20] G. R. Satchler, *Direct Nuclear Reactions* (Clarendon Press, Oxford, 1983).
[21] R. S. Mackintosh, Phys. Rev. C **88**, 054603 (2013).
[22] F. D. Becchetti and G. W. Greenlees, Phys. Rev. **182**, 1190 (1969).
[23] A. J. Koning and J. P. Delaroche, Nucl. Phys. A **713**, 231 (2003).
[24] C. A. Coulter and G. R. Satchler, Nucl. Phys. A **293**, 269 (1977).
[25] R. S. Mackintosh and S. G. Cooper, J. Phys. G: Nucl. Part. Phys. **23**, 565 (1997).
[26] L. J. Titus and F. M. Nunes, Phys. Rev. C **89**, 034609 (2014).
[27] G. H. Rawitscher, Nucl. Phys. A **475**, 519 (1987).
[28] H. Feshbach, Ann. Phys. **5**, 357 (1958); **19**, 287 (1962).
[29] H. Fiedeldey, R. Lipperheide, G. H. Rawitscher, and S. A. Sofianos, Phys. Rev. C **45**, 2885 (1992).
[30] H. S. Köhler, Nucl. Phys. A **928**, 9 (2014).